Cell Reports

Article

The PP2A phosphatase counteracts the function of the 9-1-1 axis in checkpoint activation

Graphical abstract

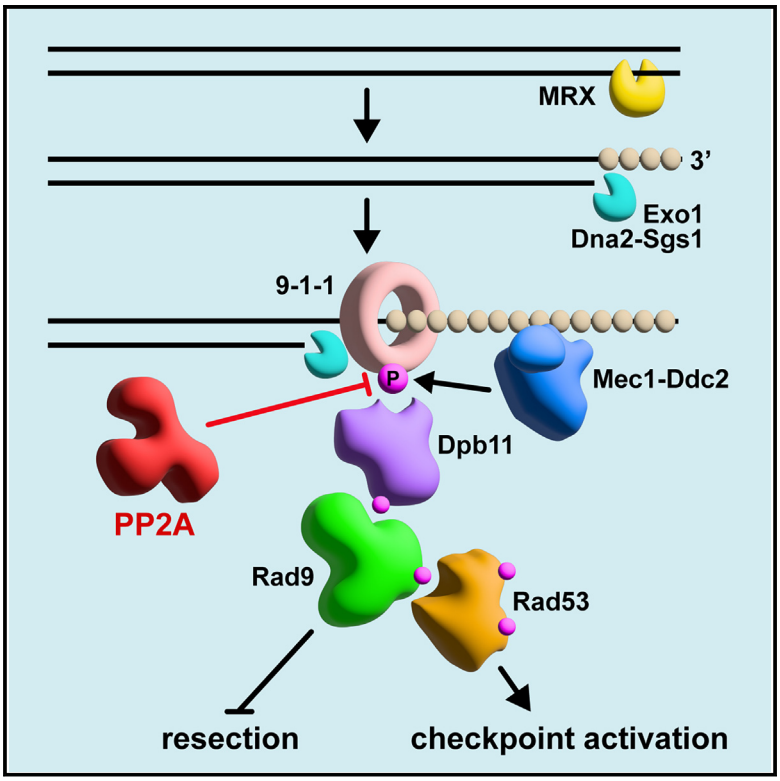

Authors

Erika Casari, Paolo Pizzul, Carlo Rinaldi, Marco Gnugnoli, Michela Clerici, Maria Pia Longhese

Correspondence

mariapia.longhese@unimib.it

In brief

Casari et al. show that the PP2A phosphatase dampens checkpoint signaling by the 9-1-1 axis. This anti-checkpoint function depends on the ability of the Cdc55 PP2A subunit to counteract Ddc1-Dpb11 complex formation by preventing Dpb11 recognition of Ddc1 phosphorylated on Thr602.

Highlights

- The PP2A phosphatase negatively regulates the 9-1-1 checkpoint axis
- The lack of this function impairs checkpoint recovery and double-strand break resection
- The Cdc55 PP2A subunit interacts with Ddc1
- Cdc55 counteracts Ddc1-Dpb11 interaction by preventing Ddc1 Thr602 phosphorylation

Casari et al., 2023, Cell Reports *42*, 113360
November 28, 2023
https://doi.org/10.1016/j.celrep.2023.113360

CellPress

Cell Reports

CellPress
OPEN ACCESS

Article

The PP2A phosphatase counteracts the function of the 9-1-1 axis in checkpoint activation

Erika Casari,[1] Paolo Pizzul,[1] Carlo Rinaldi,[1] Marco Gnugnoli,[1] Michela Clerici,[1] and Maria Pia Longhese[1,2,*]
[1]Dipartimento di Biotecnologie e Bioscienze, Università degli Studi di Milano-Bicocca, 20126 Milano, Italy
[2]Lead contact
*Correspondence: mariapia.longhese@unimib.it
https://doi.org/10.1016/j.celrep.2023.113360

SUMMARY

DNA damage elicits a checkpoint response depending on the Mec1/ATR kinase, which detects the presence of single-stranded DNA and activates the effector kinase Rad53/CHK2. In *Saccharomyces cerevisiae*, one of the signaling circuits leading to Rad53 activation involves the evolutionarily conserved 9-1-1 complex, which acts as a platform for the binding of Dpb11 and Rad9 (referred to as the 9-1-1 axis) to generate a protein complex that allows Mec1 activation. By examining the effects of both loss-of-function and hypermorphic mutations, here, we show that the Cdc55 and Tpd3 subunits of the PP2A phosphatase counteract activation of the 9-1-1 axis. The lack of this inhibitory function results in DNA-damage sensitivity, sustained checkpoint-mediated cell-cycle arrest, and impaired resection of DNA double-strand breaks. This PP2A anti-checkpoint role depends on the capacity of Cdc55 to interact with Ddc1 and to counteract Ddc1-Dpb11 complex formation by preventing Dpb11 recognition of Ddc1 phosphorylated on Thr602.

INTRODUCTION

DNA double-strand breaks (DSBs) undergo nucleolytic degradation (resection) of their 5′-ending strands to generate 3′-ended single-stranded DNA (ssDNA) overhangs that initiate DSB repair by homologous recombination (HR).[1] DSB resection involves sequential engagement of short-range and long-range nucleases.[2] Short-range nucleases comprise the Mre11 subunit of the Mre11-Rad50-Xrs2/NBS1 (MRX/N) complex that, aided by the Sae2 protein (CtIP in mammals), catalyzes a cleavage of the 5′-terminated DNA strand at each DSB end.[3] This step is followed by resection of the 5′ strands away from the DSB, which is carried out by either the Exo1 or Dna2 long-range nuclease, the latter requiring the helicase Sgs1 (WRN or BLM in mammals).[4–12]

Generation of RPA-coated ssDNA at the DSB ends also activates a checkpoint response that depends on the apical Mec1 kinase (ATR in mammals),[13] which activates the downstream protein kinases Rad53 and Chk1 (CHK2 and CHK1 in mammals, respectively). In budding yeast, the transfer of phosphorylation from apical to downstream checkpoint kinases requires the Rad9 protein (53BP1 in mammals), which acts both as an adaptor between Mec1 and Rad53 and as a scaffold to promote Rad53 autophosphorylation and activation.[14–17]

In both yeast and mammals, the Mec1/ATR interacting protein Ddc2 (ATRIP in mammals) is needed to allow Mec1/ATR recruitment to replication protein A (RPA)-coated ssDNA.[13,18,19] Full Mec1 activation requires the ring-shaped heterotrimer Ddc1-Mec3-Rad17 (RAD9-HUS1-RAD1 in mammals), hereafter referred to as 9-1-1, which is loaded at double-stranded DNA (dsDNA) adjacent to ssDNA by the Rad24-RFC clamp loader. The 9-1-1 complex serves as a platform for the association of additional proteins (referred to as the 9-1-1 axis), such as Dpb11 (TopBP1 in mammals) and Rad9, which are critically required for recruitment, phosphorylation, and activation of the effector kinase Rad53.[20–26] In *Saccharomyces cerevisiae*, the interaction between 9-1-1 and Dpb11 is dependent on Mec1-mediated phosphorylation of Ddc1 on Thr602, and this phospho-dependent Dpb11-Ddc1 association is conserved in mammals.[24–27] Rad9 recruitment to DSBs by the 9-1-1 complex also negatively regulates DSB resection by inhibiting the activity of the long-range resection nucleases Exo1 and Dna2-Sgs1.[28–33]

It is noteworthy that abrogation of long-range resection due to the lack of both Exo1 and Sgs1 reduces the activation of the 9-1-1 checkpoint axis in response to a single site-specific DSB.[34] By contrast, the 9-1-1 checkpoint response is enhanced when *exo1*Δ *sgs1*Δ cells are exposed to DNA-damaging agents.[35] Given that the ssDNA generated at the DSB ends in *exo1*Δ *sgs1*Δ cells is limited to 100–300 nucleotides,[4,5] the amount produced at a single DSB may not reach the necessary threshold for Mec1 activation. On the other hand, when *exo1*Δ *sgs1*Δ cells are subjected to genotoxic agents, the MRX-mediated processing of multiple DSBs can lead to an accumulation of several 5′-recessed dsDNA/ssDNA junctions that are avidly bound by the 9-1-1 complex.[21,34–37] The sustained activation of the 9-1-1 axis in *exo1*Δ *sgs1*Δ cells following genotoxic exposure contributes to increase their DNA-damage sensitivity. In fact, when the 9-1-1 complex fails to recruit Dpb11 and Rad9 to the damaged sites, the DNA-damage resistance of *exo1*Δ *sgs1*Δ cells is partially restored.[35]

Once DNA lesions are repaired, cells resume cell-cycle progression by downregulating the checkpoint response. The appearance of unphosphorylated Rad53, which accompanies

checkpoint deactivation,[38] does not require protein synthesis, suggesting that activated Rad53 is dephosphorylated, not degraded.[39] Depending on the type of DNA lesions, different phosphatases have been implicated in Rad53 dephosphorylation and checkpoint deactivation. In particular, the PP2C phosphatases Ptc2 and Ptc3 have been shown to dephosphorylate Rad53 after generation of a persistent DSB,[40,41] whereas the PP1 phosphatase Glc7 promotes Rad53 deactivation after exposure to hydroxyurea.[42] The PP4 phosphatase Pph3, when complexed with Psy2, dephosphorylates Rad53 upon recovery from treatment with methyl methanesulfonate,[43,44] with Ptc2 and Ptc3 compensating for Pph3 loss, and vice versa.[45,46] Furthermore, Pph3 physically interacts with Mec1-Ddc2,[47] and it has been implicated in dephosphorylation of Mec1 targets, such as Zip1,[48] Cdc13,[49] Cbf1,[50] histone H2A,[51] and Mec1 itself.[47] Finally, the PP2A phosphatase has been reported to attenuate Mec1 signaling activity in *S. cerevisiae* cells experiencing replication stress[52] and to show activity toward mammalian ATM, p53, CHK1, CHK2, and H2A proteins.[53–58] In *S. cerevisiae*, PP2A consists of a scaffold A subunit (Tpd3), a regulatory B subunit (Cdc55, Rts1, or Rts3), and two interchangeable catalytic C subunits (Pph21 and Pph22).[59] Among them, the regulatory B subunit primarily dictates cellular localization and PP2A substrate specificity.[60]

Here, we show that hypermorphic mutations in the PP2A subunits Cdc55 and Tpd3 downregulate the 9-1-1 checkpoint axis, whereas the lack of Cdc55 or Tpd3 hyperactivates it. This function relies on the ability of Cdc55 to interact with Ddc1 and to prevent Ddc1-Dpb11 complex formation and therefore Rad9 recruitment to damaged DNA. Decreased Rad9 association with DSBs by Cdc55 and Tpd3 not only impairs checkpoint activation but also increases the efficiency of DSB resection. We propose that PP2A negatively regulates checkpoint signaling by the 9-1-1 complex, avoiding persistent checkpoint-mediated cell-cycle arrest and DNA-damage-induced cell death.

RESULTS

The *cdc55-Q335E* and *tpd3-I384N* alleles suppress the DNA-damage sensitivity of *exo1*Δ *sgs1*Δ cells

We have previously described a genetic screen for extragenic mutations that suppressed the sensitivity to DNA-damaging agents of cells lacking both Exo1 and Sgs1, which are required to allow long-range resection.[35] DNA-damage resistance of two suppressor mutants was due to single base pair substitutions in the genes encoding Rad24 and Dpb11.[35] Genome-wide sequencing and classical genetic analyses of two other non-allelic suppressors allowed us to establish that the suppressing mutations hit two different genes: *CDC55* and *TPD3*, which encode the regulatory and the scaffolding subunits of the protein phosphatase PP2A, respectively. While the *CDC55* suppressor carried the missense mutation of Gln335 to Glu, *TPD3* carried the substitution of Ile384 to Asn. Both *cdc55-Q335E* and *tpd3-I384N* suppressed the sensitivity of *exo1*Δ *sgs1*Δ cells to the topoisomerase poison camptothecin (CPT) and to the DSB-inducing agent phleomycin (phleo) (Figure 1A). The suppression exerted by either *cdc55-Q335E* or *tpd3-I384N* turned out to be specific for *exo1*Δ *sgs1*Δ cells, as the same mutations did not suppress the DNA-damage sensitivity of *sae2*Δ cells (Figure 1B).

To evaluate the possibility that *exo1*Δ *sgs1*Δ suppression by *cdc55-Q335E* and *tpd3-I384N* could depend on reduced Cdc55 or Tpd3 activity, we analyzed the consequence of *CDC55* or *TPD3* deletion in *exo1*Δ *sgs1*Δ cells. Tetrad dissection from triple-heterozygous diploid cells showed that the lack of Cdc55 or Tpd3 causes synthetic lethality when Exo1 and Sgs1 are concomitantly absent. In fact, both *cdc55*Δ *exo1*Δ *sgs1*Δ (Figure 1C) and *tpd3*Δ *exo1*Δ *sgs1*Δ (Figure 1D) spores are unable to form colonies, whereas *cdc55*Δ and *tpd3*Δ spores can generate colonies, although colonies from *tpd3*Δ spores were smaller than those derived from the wild-type spores (Figure 1D). The finding that the lack of Cdc55 or Tpd3 is lethal in *exo1*Δ *sgs1*Δ cells suggests that the suppression of the DNA-damage sensitivity of *exo1*Δ *sgs1*Δ cells exerted by the *cdc55-Q335E* and *tpd3-I384N* mutations may result from a loss of function toward specific substrates or may not be linked to a decrease of Cdc55 or Tpd3 activity.

The ability of the two alleles to suppress the sensitivity of *exo1*Δ *sgs1*Δ cells to genotoxic agents was dominant, as *CDC55/cdc55-Q335E exo1*Δ*/exo1*Δ *sgs1*Δ*/sgs1*Δ diploid cells were less sensitive to phleomycin compared with *CDC55/CDC55 exo1*Δ*/exo1*Δ *sgs1*Δ*/sgs1*Δ diploid cells (Figure 1E). Similar results have been obtained with the *tpd3-I384N* mutation (Figure 1F).

Suppression of the DNA-damage sensitivity of *exo1*Δ *sgs1*Δ cells is due to the inhibition of the 9-1-1 axis

The lack of both Exo1 and Sgs1 hyperactivates a checkpoint in response to genotoxic treatments that depends on the 9-1-1 complex, which recruits the scaffold proteins Dpb11 and Rad9 (referred to as the 9-1-1 axis) via an interaction between Ddc1 phosphorylated on Thr602 and Dpb11.[35] In fact, Rad53 phosphorylation dramatically increased in phleomycin-treated *exo1*Δ *sgs1*Δ cells compared to wild-type cells, whereas *exo1*Δ *sgs1*Δ cells expressing the *ddc1-T602A* allele, where Thr602 was substituted with a non-phosphorylatable alanine residue, decreased Rad53 phosphorylation to levels observed in both wild-type and *ddc1-T602A* single-mutant cells (Figure 2A). In contrast, Rad53 phosphorylation remained high when *exo1*Δ *sgs1*Δ cells carried the *ddc1-T602E* allele, where Thr602 was replaced by glutamic acid that should mimic constitutive phosphorylation by imparting a negative charge to the protein (Figure 2A).

As the physical interaction between Ddc1 and Dpb11 has been demonstrated by using two-hybrid assays,[20,25] to confirm the requirement of Thr602 phosphorylation for Ddc1-Dpb11 interaction, we used a two-hybrid approach in phleomycin-treated cells expressing Dpb11 together with wild-type Ddc1, $Ddc1^{T602A}$, or $Ddc1^{T602E}$. We found that Ddc1 interacts with Dpb11, and this interaction decreased to background levels when Ddc1 had the T602A mutation, whereas it was unaffected when Ddc1 carried the T602E mutation (Figure 2B), thus underscoring the importance of phosphorylation at this site for the Ddc1-Dpb11 interaction.

We have previously shown that the persistent activation of the 9-1-1 checkpoint axis contributes to sensitize *exo1*Δ *sgs1*Δ cells

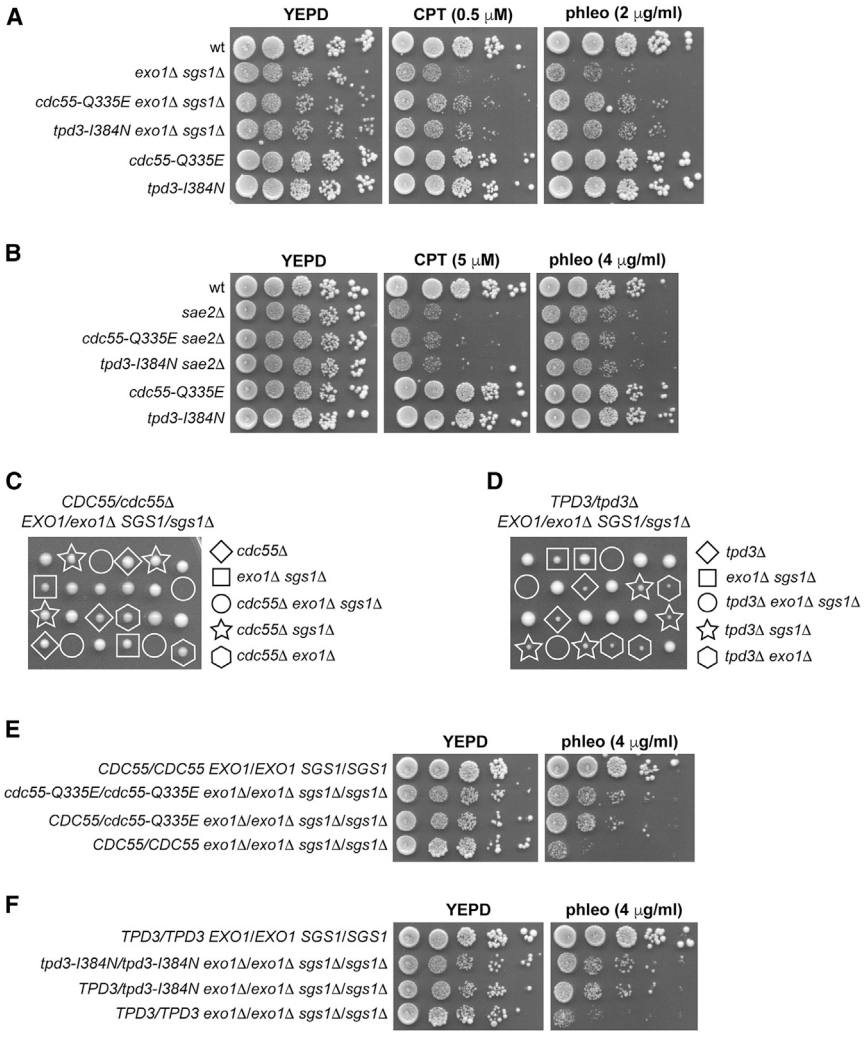

Figure 1. *cdc55-Q335E* and *tpd3-I384N* partially suppress the DNA-damage sensitivity of *exo1Δ sgs1Δ* cells, whereas *cdc55Δ* and *tpd3Δ* are lethal in *exo1Δ sgs1Δ* cells

(A and B) Exponentially growing cultures were serially diluted (1:10), and each dilution was spotted out onto yeast extract-peptone-glucose (YEPD) plates with or without CPT or phleomycin.

(C and D) Meiotic tetrads were dissected on YEPD plates that were incubated at 25°C, followed by spore genotyping.

(E and F) Exponentially growing cultures were serially diluted (1:10), and each dilution was spotted out onto YEPD plates with or without phleomycin.

to genotoxic agents, as the *ddc1-T602A* allele partially suppressed the DNA-damage sensitivity of *exo1Δ sgs1Δ* cells.[35] Thus, we investigated whether the *cdc55-Q335E* and *tpd3-I384N* alleles can partially restore DNA-damage resistance of *exo1Δ sgs1Δ* cells by downregulating the checkpoint response. The presence of either *cdc55-Q335E* or *tpd3-I384N* decreased Rad53 phosphorylation in phleomycin-treated *exo1Δ sgs1Δ* cells, but not in *exo1Δ sgs1Δ* cells carrying the *ddc1-T602E* mutation that mimics constitutive T602 phosphorylation (Figure 2C), suggesting that checkpoint downregulation by the *cdc55-Q335E* and *tpd3-I384N* mutations requires T602 dephosphorylation. Furthermore, the *ddc1-T602A* mutation suppressed the DNA-damage sensitivity of *exo1Δ sgs1Δ* cells, and the presence of *cdc55-Q335E* did not increase further the DNA-damage resistance of *ddc1-T602A exo1Δ sgs1Δ* (Figure 2D). This finding indicates that the *cdc55-Q335E* and *ddc1-T602A* mutations exert their action in the same pathway, suggesting that the increased DNA-damage resistance of *cdc55-Q335E exo1Δ sgs1Δ* cells is due to the downregulation of the 9-1-1 axis. Finally, activation of the 9-1-1 checkpoint response can account for the loss of viability of *cdc55Δ exo1Δ sgs1Δ* and *tpd3Δ exo1Δ sgs1Δ* cells, as the *ddc1-T602A* allele restored viability of *cdc55Δ exo1Δ sgs1Δ* (Figure 2E) and *tpd3Δ exo1Δ sgs1Δ* spores (Figure 2F).

Dampening activation of the 9-1-1 axis by Cdc55 and Tpd3 promotes checkpoint recovery and DNA-damage resistance

To assess whether the role of Cdc55 and Tpd3 in the downregulation of the 9-1-1-mediated checkpoint is physiologically relevant also in a wild-type context, we analyzed Rad53 phosphorylation after phleomycin exposure in cells lacking Cdc55 or Tpd3. Deletion of *CDC55* or *TPD3* dramatically increased phleomycin-induced Rad53 phosphorylation (Figure 3A). Abrogation of the Ddc1-Dpb11 interaction by expressing the *ddc1-T602A* allele decreased Rad53 phosphorylation of *cdc55Δ* and *tpd3Δ* cells to levels observed in both wild-type and *ddc1-T602A* cells (Figure 3A), indicating that Cdc55 and Tpd3 downregulate a checkpoint response that is dependent on the 9-1-1 axis.

Next, to evaluate whether the enhanced activation of the 9-1-1-mediated checkpoint sensitizes *cdc55Δ* and *tpd3Δ* cells to DNA-damaging agents, we examined the DNA-damage sensitivity of *cdc55Δ* cells, which do not show growth defects when not exposed to genotoxic stress. As shown in Figure 3B, *cdc55Δ* cells were hypersensitive to both CPT and phleomycin, and the presence of the *ddc1-T602A* mutation suppressed this DNA-damage sensitivity, indicating that Cdc55 supports DNA-damage resistance by negatively controlling 9-1-1-mediated checkpoint signaling.

As the lack of Cdc55 leads to checkpoint hyperactivation and DNA-damage hypersensitivity that are both suppressed by the *ddc1-T602A* allele (Figure 3), we investigated whether Cdc55 and Tpd3 are required to recover from a DNA-damage-induced checkpoint. To this purpose, cells were treated with phleomycin

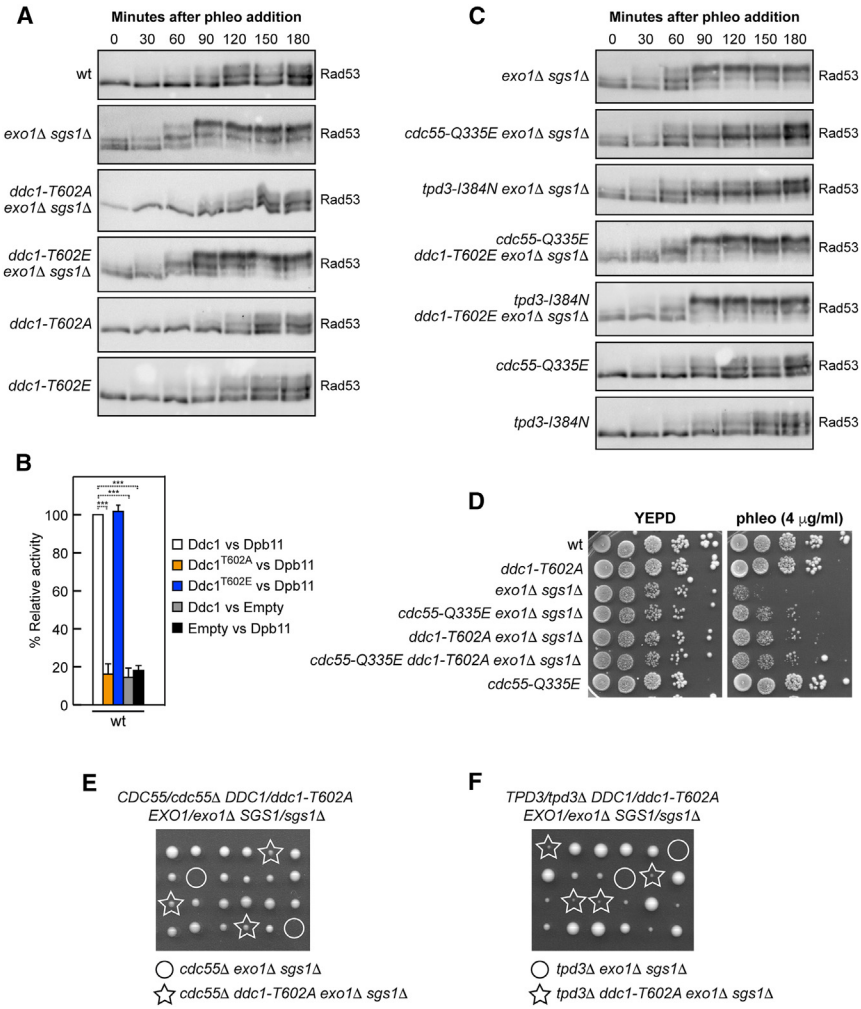

Figure 2. *cdc55-Q335E* and *tpd3-I384N* dampen hyperactivation of the 9-1-1 axis in *exo1Δ sgs1Δ* cells

(A) Phleomycin (10 μg/mL) was added to exponentially growing cells, and protein extracts were analyzed by western blot using anti-Rad53 antibodies. This experiment was performed independently three times with similar results.

(B) Two-hybrid interactions between Dpb11 and Ddc1, Ddc1^{T602A}, or Ddc1^{T602E}. Cells were treated with phleomycin (10 μg/mL) before measuring relative β-galactosidase activity with the ONPG assay. The Ddc1-Dpb11 interaction was set up to 100%. The mean values of three independent experiments are represented with error bars denoting SD. ***$p < 0.005$ (Student's t test).

(C) Phleomycin (10 μg/mL) was added to exponentially growing cells, and protein extracts were analyzed by western blot using anti-Rad53 antibodies. This experiment was performed independently three times with similar results.

(D) Exponentially growing cultures were serially diluted (1:10), and each dilution was spotted out onto YEPD plates with or without phleomycin.

(E and F) Meiotic tetrads were dissected on YEPD plates that were incubated at 25°C followed by spore genotyping.

before transferring them to a medium lacking phleomycin to analyze Rad53 phosphorylation and microcolony formation. Because the activation of the 9-1-1-mediated checkpoint occurs preferentially in the G2 phase of the cell cycle,[26] phleomycin treatment was performed in cells arrested in G2 with nocodazole. As shown in Figure 4A, Rad53-phosphorylated bands started to disappear 90 min after phleomycin removal in wild-type cells, whereas they persisted longer in both *cdc55*Δ and *tpd3*Δ cells, indicating a recovery defect. The sustained Rad53 activation in *cdc55*Δ and *tpd3*Δ cells appears to correlate with a prolonged cell-cycle arrest. In fact, wild-type cells accumulated colonies with more than two cells faster than *cdc55*Δ and *tpd3*Δ cells, of which approximately 40% were still arrested as large-budded cells (2 cells) 5 h after phleomycin removal (Figure 4B). By contrast, *cdc55-Q335E* and *tpd3-I384N* cells decreased Rad53 phosphorylation and formed microcolonies with more than two cells slightly faster than wild-type cells and with kinetics similar to that of *ddc1-T602A* cells (Figures 4A and 4B).

Again, the recovery defect imparted by *CDC55* or *TPD3* deletion is due to the persistent activation of the 9-1-1-dependent checkpoint. In fact, abrogation of the Ddc1-Dpb11 interaction suppresses the recovery defect of *cdc55*Δ and *tpd3*Δ cells, as Rad53 dephosphorylation (Figure 4A) and microcolony formation (Figure 4B) occurred faster in *cdc55*Δ *ddc1-T602A* and *tpd3*Δ *ddc1-T602A* cells than in *cdc55*Δ and *tpd3*Δ cells and with kinetics similar to that of *ddc1-T602A* single-mutant cells. Furthermore, mimicking constitutive Ddc1 Thr602 phosphorylation by expressing the *ddc1-T602E* allele hinders the rapid checkpoint recovery of *cdc55-Q335E* and *tpd3-I384N* cells, as Rad53 dephosphorylation (Figure 4A) and microcolony formation (Figure 4B) occurred later in *cdc55-Q335E ddc1-T602E* and *tpd3-I384N ddc1-T602E* cells than in *cdc55-Q335E* and *tpd3-I384N* cells and with kinetics similar to that of *ddc1-T602E* single-mutant cells. These results suggest that Cdc55 and Tpd3 promote recovery from the 9-1-1-mediated checkpoint and that this function is increased by the *cdc55-Q335E* and *tpd3-I384N* mutations.

Cdc55 promotes DSB resection by limiting Rad9 association to DSBs

The 9-1-1 complex was shown to inhibit DSB processing by recruiting Rad9, which acts as a barrier against the resection activity of the long-range resection nucleases Exo1 and Dna2-Sgs1.[28–33] Because Cdc55 and Tpd3 downregulate the 9-1-1-dependent checkpoint response, we investigated the potential role of Cdc55 in regulating DSB resection using JKM139 derivative strains, where a single irreparable DSB can be generated by expressing the *HO* endonuclease gene.[61] In this strain, the

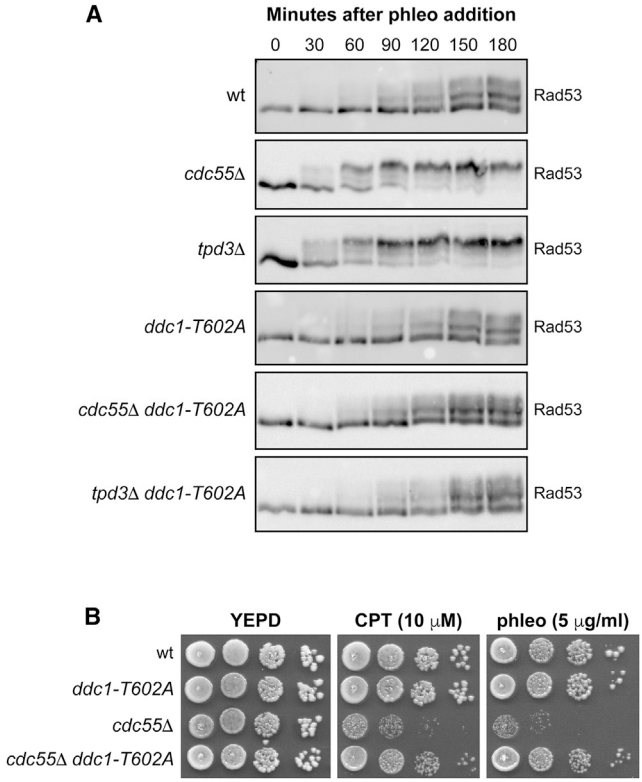

Figure 3. The lack of Cdc55 or Tpd3 causes Rad53 hyperactivation and DNA-damage sensitivity in a manner dependent on Ddc1 Thr602 phosphorylation

(A) Phleomycin (10 μg/mL) was added to exponentially growing cells, and protein extracts were analyzed by western blot using anti-Rad53 antibodies. This experiment was performed independently three times with similar results. (B) Exponentially growing cultures were serially diluted (1:10), and each dilution was spotted out onto YEPD plates with or without CPT or phleomycin.

addition of galactose induces the expression of *HO*, which catalyzes a single DSB at the *MAT* locus that cannot be repaired by HR due to the deletion of both the homologous donor sequences *HML* and *HMR*.[61] Because ssDNA cannot be cleaved by restriction enzymes, we evaluated the generation of ssDNA by examining its resistance to cleavage as resection progresses past the *Ssp*I restriction sites situated at varying distances from the HO cut site (Figure 5A). The presence of *Ssp*I-resistant ssDNA can be detected as the appearance of longer restriction fragments (r1–r7) after denaturing gel electrophoresis of *Ssp*I-digested genomic DNA and subsequent hybridization with a probe that anneals to the unresected strand on one side of the DSB.

When *HO* was induced by galactose addition to exponentially growing cells, the resection products were observed to appear more efficiently in galactose-induced *cdc55-Q335E* cells than in wild-type cells (Figures 5B and 5C), suggesting a role of Cdc55 in the regulation of DSB resection. To confirm this finding, we tested whether DSB resection is impaired in *cdc55*Δ cells. Because the detection of *Ssp*I-resistant ssDNA by southern blotting can only assess resection events that extend beyond the *Ssp*I site located 0.9 kb from the HO cut site (Figure 5A), we employed a quantitative PCR-based approach to detect the generation of restriction-enzyme-resistant ssDNA in proximity to the HO cut site.[62] This method relies not only on the *Ssp*I cut sites used in the southern blot but also on two *Rsa*I cut sites situated at distances of 0.15 and 0.65 kb from the HO-induced DSB (Figure 5A). If resection has extended beyond these recognition sites, the DNA region would remain uncut and would be amplified by PCR using primers flanking the restriction site. We observed that *CDC55* deletion did not impact the generation of ssDNA at DNA regions in close proximity to the HO cut site (0.15 kb), whereas a decrease in ssDNA generation can be detected at more distant sites (0.65, 0.9, 1.7, and 3.5 kb) (Figure 5D), indicating that Cdc55 plays a role in promoting long-range resection.

Long-range resection involves Exo1 and Dna2-Sgs1, whose resection activities are inhibited by Rad9.[28,29,31–33] In the absence of both Exo1 and Sgs1, the generation of ssDNA relies on the Mre11 nuclease activity and is constrained to 100–300 nucleotides from the DSB ends.[4,5,35,63] As expected, ssDNA in *exo1*Δ *sgs1*Δ cells can be detected in close proximity to the HO cut site (0.15 kb) but not at more distant sites (0.65 and 0.9 kb) (Figure 5E). Consistent with a role of Cdc55 in promoting long-range resection, the *cdc55-Q335E* mutation was unable to suppress the resection defect of *exo1*Δ *sgs1*Δ cells (Figure 5E), indicating that the increased resection of *cdc55-Q335E* cells requires the presence of one or both of Exo1 and Sgs1. This finding also implies that the suppression of the DNA-damage sensitivity of *exo1*Δ *sgs1*Δ cells by *cdc55-Q335E* is not due to a restored DSB resection.

Because Cdc55 counteracts the signaling activity of the 9-1-1 complex, which has been shown to inhibit DSB resection by recruiting Rad9 at DSBs,[30] the lack of Cdc55 might hinder DSB resection by increasing Rad9 binding/persistence at DSBs. Conversely, the *cdc55-Q335E* allele might enhance DSB resection by reducing Rad9 binding/persistence at DSBs. Although protein extracts contained similar amounts of Rad9 protein (Figure S1), the amount of Rad9 bound at the HO-induced DSB detected by chromatin immunoprecipitation (ChIP) and quantitative PCR was increased in *cdc55*Δ cells, whereas it was decreased in both *cdc55-Q335E* and *tpd3-I384N* cells (Figure 5F). This finding suggests that Cdc55 promotes DSB resection by negatively controlling Rad9 association with DSBs.

Cdc55 binding to Ddc1 counteracts Ddc1-Dpb11 interaction

As reported for the human orthologs, Cdc55 has a β-propeller structure composed of seven WD40 repeats,[64] whereas yeast Tpd3 has a solenoid structure composed of 15 HEAT (huntingtin-elongation-A subunit-TOR) motifs.[65] By analyzing the yeast PP2A trimeric structure predicted by AlphaFold2-Multimer,[66] we found that the identified Cdc55 Gln335 residue is localized on the loop between WD5 and WD6 domains (Figure 6A). The Tpd3 Ile384 residue is located on the HEAT 9 domain (Figure 6A), and its mutation to Asn introduces a hydrophilic residue in a hydrophobic region. In both cases, predicting the effects of the mutations on the structure of the PP2A complex is challenging.

Activation of the 9-1-1 axis depends on Ddc1 binding to Dpb11, a step that requires DNA-damage-induced phosphorylation of Ddc1 Thr602 by Mec1.[20,25,26] Ddc1 contains eight

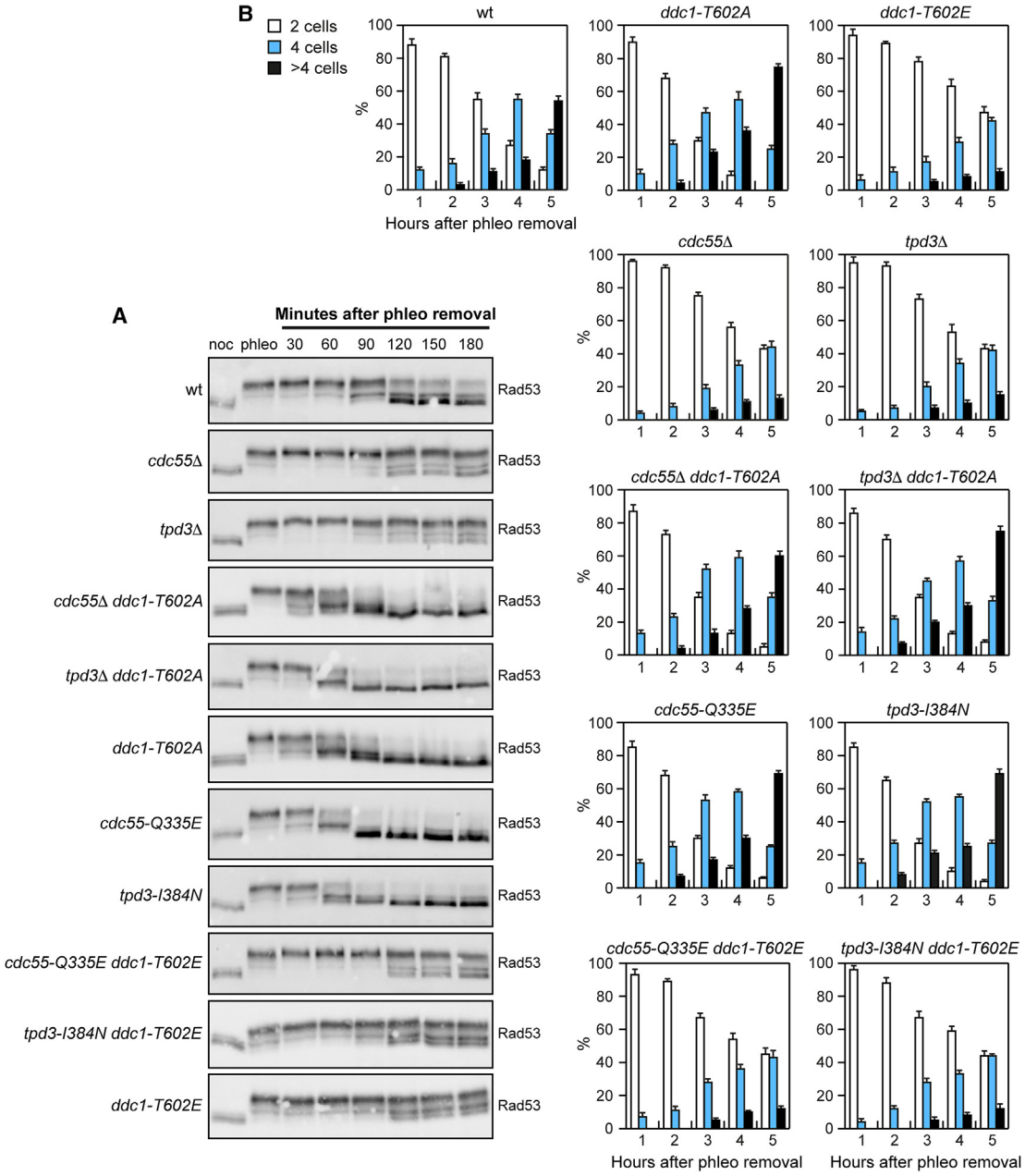

Figure 4. Cdc55 and Tpd3 promote recovery from a 9-1-1-dependent checkpoint

(A) Phleomycin (60 μg/mL) was added to nocodazole-arrested cells (indicated as noc). After 2 h in the presence of phleomycin (indicated as phleo), cells were transferred to medium lacking both phleomycin and nocodazole. Aliquots of each culture were harvested at the indicated times after phleomycin removal to detect Rad53 by western blot analysis. This experiment was performed independently three times with similar results.

(B) Phleomycin (60 μg/mL) was added to nocodazole-arrested cells. After 2 h, cells were spotted on plates lacking both phleomycin and nocodazole. At the indicated time points, 200 cells for each strain were analyzed to determine the frequency of large-budded cells (2 cells) and of cells forming microcolonies of 4 or more cells. The experiment was independently repeated three times, and the mean values are represented with error bars denoting SD.

potential Mec1 phosphorylation sites, with one of these sites being T602.[25] We have previously shown that DNA-damage-induced Ddc1 phosphorylation results in a decrease of its electrophoretic mobility that is detectable by western blot on trichloroacetic acid (TCA) extracts, which preserve phosphorylation events better than other protein extraction methods.[67] A mutant variant of Ddc1 in which all eight phosphorylatable residues are changed to alanine abolishes the mobility shift of Ddc1.[25] However, it has not been determined which of these sites are responsible for this effect. Because our results indicate a role for Cdc55 in counteracting activation of the 9-1-1 checkpoint axis, we analyzed Ddc1 electrophoretic mobility upon

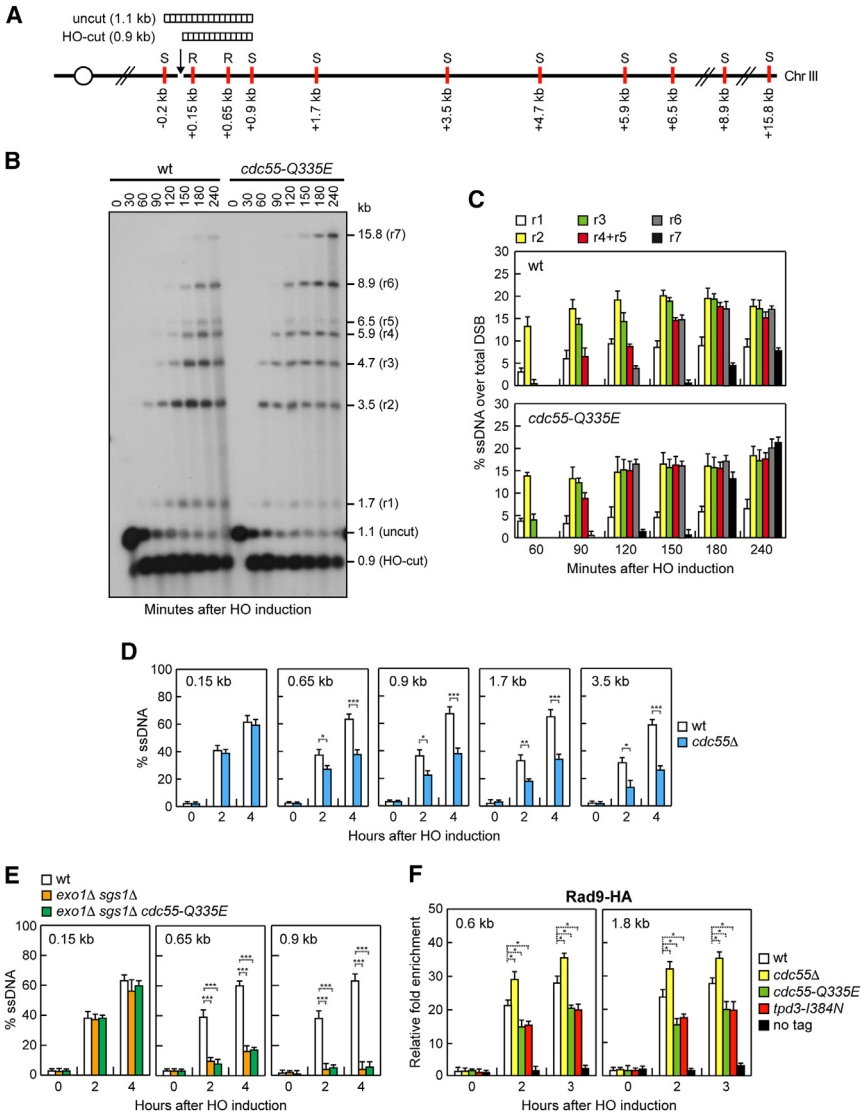

Figure 5. Cdc55 inhibits DSB resection by counteracting Rad9 association with DSBs

(A) Schematic representation of the *MAT* locus and the distance of *Rsa*I (R) and *Ssp*I (S) restriction sites from the HO cut site. The DNA fragments detected in (B) before (uncut) and after HO cleavage (HO cut) are also indicated.

(B) YEPR exponentially growing cell cultures were transferred to YEPRG at time zero to induce *HO* expression. *Ssp*I-digested genomic DNA separated on alkaline agarose gel was hybridized with a single-stranded *MAT* probe that anneals with the unresected strand. 5′-3′ resection progressively eliminates *Ssp*I sites, producing longer *Ssp*I fragments (r1–r7) detected by the probe.

(C) Densitometric analysis. The experiment, as in (B), was independently repeated three times, and the mean values are represented with error bars denoting SD.

(D and E) Quantification of ssDNA by qPCR at the indicated distances from the HO cut site. Plotted values are the mean values of three independent experiments, with error bars denoting SD. ***$p < 0.005$, **$p < 0.01$, *$p < 0.05$ (Student's t test).

(F) ChIP and qPCR. Exponentially growing YEPR cell cultures were transferred to YEPRG to induce *HO* expression, followed by ChIP analysis of the recruitment of Rad9-HA at the indicated distance from the HO cut. In all diagrams, ChIP signals were normalized for each time point to the corresponding input signal. The mean values of three independent experiments are represented, with error bars denoting SD. *$p < 0.05$ (Student's t test).

DNA damage exposure of G2-arrested cells. Ddc1 was phosphorylated after phleomycin treatment, and mutating the Ddc1 Thr602 residue to Ala dramatically reduced the Ddc1 mobility shift (Figure 6B). This finding suggests that Thr602 is the primary phosphorylation site responsible for the observed change of Ddc1 electrophoretic mobility. Alternatively, given that Thr602 is the only residue phosphorylated by Mec1 that allows Ddc1 to bind to Dpb11 and to consequently activate Mec1,[26] the lack of Thr602 phosphorylation could hinder the phosphorylation of other Ddc1 putative target sites by impairing full Mec1 activation. Phleomycin-induced Ddc1 phosphorylation dramatically decreased in *cdc55-Q335E* cells (Figure 6B). By contrast, the lack of Cdc55 increased phosphorylation of wild-type Ddc1, but not of the Ddc1^{T602A} mutant variant (Figure 6B), indicating that Cdc55 counteracts Ddc1 Thr602 phosphorylation.

Next, we investigated whether Cdc55 and Ddc1 might bind to each other by creating yeast strains that expressed epitope-tagged versions of Ddc1 and Cdc55 from their native genomic loci. Immunoprecipitation of Ddc1-HA efficiently recovered Cdc55-Myc, indicating that Ddc1 interacts with Cdc55 (Figure 6C). When Ddc1-HA was immunoprecipitated from cells expressing Cdc55^{Q335E}-Myc, an increased amount of Cdc55^{Q335E}-Myc could be detected in immunoprecipitates of Ddc1-HA (Figure 6C), indicating that the *cdc55-Q335E* mutation increases Cdc55-Ddc1 interaction.

To investigate whether the heightened Ddc1-Cdc55^{Q335E} interaction enhances the effectiveness of Ddc1 dephosphorylation either by making Ddc1 Thr602 a more favorable substrate or by shielding it from phosphorylation, we examined whether inhibition of PP2A activity in wild-type and *cdc55-Q335E* cells leads to a similar increase in Ddc1 phosphorylation. To inhibit PP2A activity, we employed okadaic acid (OA), a compound that binds to the active site of the catalytic subunit and inhibits it.[52,68–70] As activation of the 9-1-1 checkpoint axis occurs preferentially in the G2 phase of the cell cycle,[26] phleomycin treatment was performed in G2-arrested cells. When cells were treated with a high dose of phleomycin in the absence of OA and cell samples were analyzed over short time intervals, we observed a reduction of Ddc1 and Rad53 phosphorylation in *cdc55-Q335E* cells compared with the wild type (Figure 6D). In the presence of OA, Ddc1 and Rad53 phosphorylation increased in both

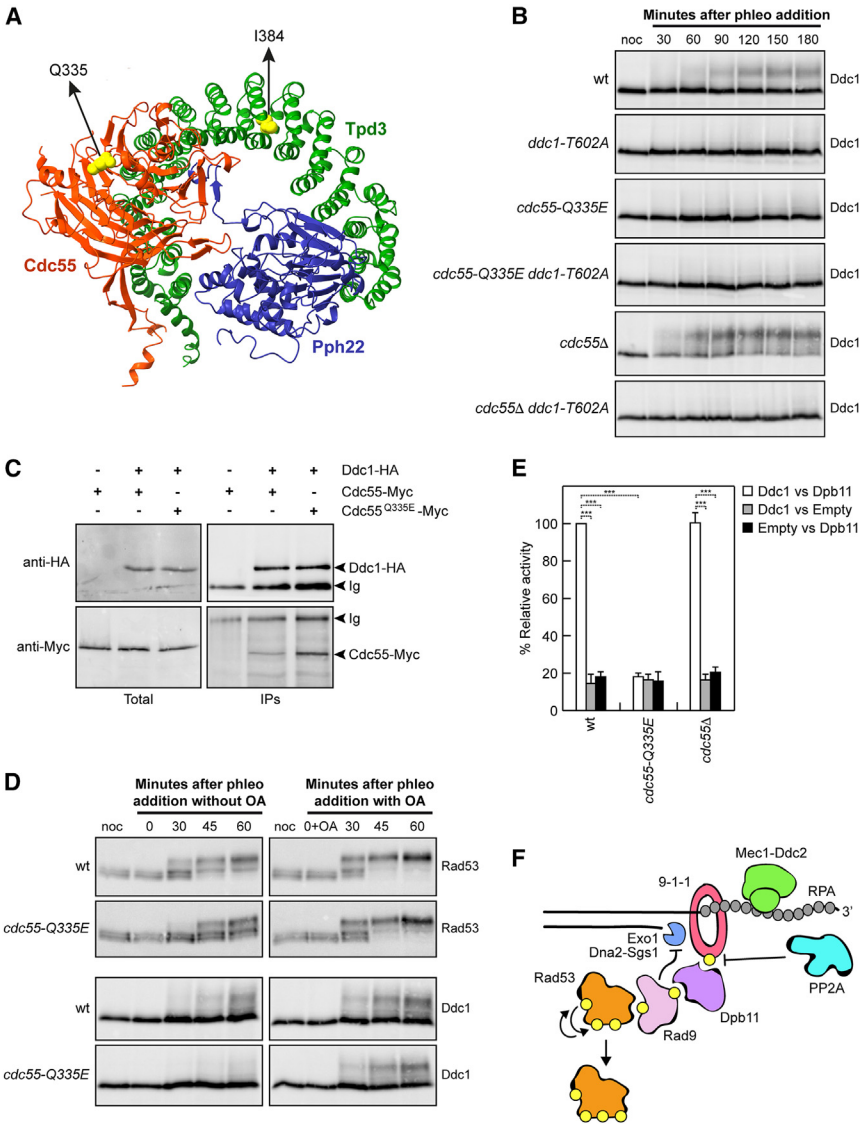

Figure 6. Cdc55 interacts with Ddc1 and inhibits Ddc1-Dpb11 interaction

(A) Predicted structure of the yeast PP2A phosphatase complex with AlphaFold2-Multimer modeling. Only the top-ranked model is shown. Pph22 is in blue, Cdc55 is in orange, and Tpd3 is in green. The Cdc55 Q335 and Tpd3 I384 residues are shown as yellow balls.

(B) Cells were arrested in G2 with nocodazole and phleomycin (10 μg/mL) was added in the presence of nocodazole. Aliquots of each culture were harvested at the indicated times after phleomycin addition to detect Ddc1 by western blot with an anti-HA antibody. This experiment was performed independently three times with similar results.

(C) Exponentially growing cells were treated with phleomycin (10 μg/mL) for 2 h. Protein extracts were analyzed by western blotting with an anti-HA or an anti-Myc antibody either directly (total) or after immunoprecipitation (immunoprecipitates [IPs]) of Ddc1-HA with an anti-HA antibody.

(D) Nocodazole-arrested cells were incubated or not with OA (3 μM). After 30 min, phleomycin (60 μg/mL) was added to both untreated and OA-treated cells in the presence of nocodazole, and aliquots of each culture were harvested at the indicated times after phleomycin addition to detect Ddc1 and Rad53 by western blot. This experiment was performed independently three times with similar results.

(E) Two-hybrid interactions between Dpb11 and Ddc1 in wild-type, *cdc55-Q335E*, and *cdc55*Δ cells. Cells were treated with phleomycin (10 μg/mL) before measuring relative β-galactosidase activity with the ONPG assay. The Ddc1-Dpb11 interaction was set up to 100%. The mean values of three independent experiments are represented with error bars denoting SD. ***p < 0.005 (Student's t test).

(F) Model for the role of PP2A in checkpoint deactivation and regulation of DSB resection. See the main text for details.

wild-type and *cdc55-Q335E* cells (Figure 6D), indicating that the enhanced ability of *cdc55-Q335E* to reduce Ddc1 phosphorylation hinges on PP2A activity. Moreover, the fact that wild-type and *cdc55-Q335E* cells in the presence of OA increase Ddc1 and Rad53 phosphorylation with similar kinetics suggests that the strengthened interaction between $Cdc55^{Q335E}$ and Ddc1 facilitates Ddc1 Thr602 dephosphorylation rather than protecting it from phosphorylation.

As Thr602 phosphorylation is required for Ddc1 to bind Dpb11, we tested whether Cdc55 binding to Ddc1 can inhibit the 9-1-1 checkpoint axis by disrupting Ddc1-Dpb11 interaction. Thus, we performed yeast two-hybrid assays between Dpb11 and Ddc1 in phleomycin-treated cells lacking Cdc55 or expressing the *cdc55-Q335E* allele. We found that Ddc1 interacts with Dpb11 in both wild-type and *cdc55*Δ cells (Figure 6E). This interaction was decreased in the presence of the $Cdc55^{Q335E}$ mutant variant (Figure 6E), which interacts more robustly with Ddc1, indicating that Cdc55 can counteract Ddc1-Dpb11 interaction, and this function is increased by the *cdc55-Q335E* mutation. These findings support the model that Cdc55, and possibly Tpd3, counteracts checkpoint signaling by interacting with Ddc1 and preventing its stable interaction with Dpb11.

DISCUSSION

Phosphorylation events frequently create binding surfaces for the regulated recruitment of interactors and the formation of multiprotein complexes. Phosphorylation of the Thr602 residue in the Ddc1 subunit of the 9-1-1 complex generates a binding site for Dpb11, which subsequently interacts with the phosphorylated form of Rad9. The assembly of this protein complex, known as the 9-1-1 axis, is crucial for transmitting the checkpoint signal from Mec1 to Rad53. The 9-1-1 checkpoint response is

especially triggered when long-range resection is disrupted due to the absence of both Exo1 and Sgs1, possibly because the MRX nuclease activity generates short recessed 5′-end structures at DNA ends that are recognized by 9-1-1, resulting in the loading of Dpb11 and Rad9.[35] Enhanced activation of the 9-1-1 axis contributes to sensitize *exo1*Δ *sgs1*Δ cells to DNA-damaging agents, as failure of 9-1-1 to recruit Dpb11 and Rad9 at DSBs partially restores DNA-damage resistance of *exo1*Δ *sgs1*Δ cells.[35]

In principle, the assembly of the 9-1-1 axis could be negatively regulated by reversing protein phosphorylation. Here, we provide genetic and biochemical evidence that the Cdc55 and Tpd3 subunits of the PP2A phosphatase dampen checkpoint signaling mediated by the 9-1-1 complex. This regulatory function occurs at the stage where Dpb11 recognizes Ddc1 phosphorylated on Thr602 (Figure 6F). In fact, expression of the hypermorphic *cdc55-Q335E* and *tpd3-I384N* mutations, which we have identified as suppressors of the DNA-damage sensitivity of *exo1*Δ *sgs1*Δ cells, results in the premature downregulation of the 9-1-1-mediated checkpoint, and this effect is abrogated in cells expressing the phospho-mimetic *ddc1-T602E* allele. Conversely, the 9-1-1-mediated checkpoint response is heightened in the absence of Cdc55 or Tpd3, and this effect is abrogated in cells expressing the non-phosphorylatable *ddc1-T602A* allele.

Hyperactivation of the 9-1-1 checkpoint axis upon PP2A inactivation increases the DNA-damage sensitivity and impairs recovery from a checkpoint-mediated cell-cycle arrest. Furthermore, in line with the fact that the 9-1-1 complex recruits Rad9 at DSBs, which, in turn, counteracts the activity of the long-range resection nucleases Exo1 and Dna2-Sgs1,[28–33] the absence of Cdc55 and Tpd3 leads to a defect in long-range resection by increasing Rad9 association with DSBs. Conversely, DSB resection is enhanced in the presence of *cdc55-Q335E*, which prematurely downregulates the 9-1-1 checkpoint and, consequently, reduces Rad9 recruitment at DSBs.

We also show that the downregulation of the 9-1-1 function relies on the ability of Cdc55 to interact with Ddc1 and to counteract Ddc1-Dpb11 complex formation. This function is exerted at the level of Dpb11 recognition of Ddc1 phosphorylated on Thr602, a step that is required for the assembly of the Dpb11-Ddc1 complex (Figure 6F).[24–26] Interestingly, the Cdc55^{Q335E} mutant variant, which possesses an increased ability to inhibit Ddc1-Dpb11 complex formation and Ddc1 phosphorylation, exhibits a stronger interaction with Ddc1. The finding that Ddc1 phosphorylation increases with similar kinetics in wild-type and *cdc55-Q335E* cells after inhibition of PP2A catalytic activity suggests that the stronger Ddc1-Cdc55^{Q335E} interaction facilitates Ddc1 Thr602 dephosphorylation rather than protecting it from phosphorylation by the Mec1 protein kinase. As Cdc55 is responsible for determining PP2A substrate specificity, it remains to be established whether the *cdc55-Q335E* mutation is specific to Ddc1 or if it could enhance dephosphorylation of other substrates.

In conclusion, we propose that PP2A negatively regulates checkpoint signaling by the 9-1-1 complex, limiting Rad9 function in checkpoint activation and resection of DNA DSBs. Because both PP2A and the 9-1-1 axis are evolutionarily conserved, it will be of interest to investigate whether the PP2A phosphatase plays a similar role in mammals to reverse DNA-damage-induced signaling events once DNA repair is completed, thus avoiding aberrant DNA-damage checkpoint activation.

Limitations of the study

We showed that PP2A dampens checkpoint signaling through the 9-1-1 axis. However, we have not elucidated the molecular mechanism through which the hypermorphic *cdc55-Q335E* and *tpd3-I384N* mutations enhance PP2A activity on Ddc1 Thr602. Although we propose that the increased Ddc1-Cdc55^{Q335E} binding renders Thr602 a more favorable substrate for dephosphorylation, the underlying molecular mechanism is still unknown. The fact that Ddc1 is a disordered protein makes it challenging to study the impact of the *cdc55-Q335E* mutation on the interaction interface between Ddc1 and Cdc55, as well as the effect of the *tpd3-I384N* mutations on Ddc1 dephosphorylation. Furthermore, it remains to be investigated whether the *cdc55-Q335E* and *tpd3-I384N* mutations represent gain-of-function mutations with regards to Ddc1 or if they can enhance dephosphorylation of other substrates. Given the limited knowledge of substrate recognition, unraveling the molecular mechanisms behind the effects of these two mutations could provide valuable insights to understand how PP2A interacts with its substrates and how specific phosphorylated sites are positioned for dephosphorylation.

STAR★METHODS

Detailed methods are provided in the online version of this paper and include the following:

- KEY RESOURCES TABLE
- RESOURCE AVAILABILITY
  - Lead contact
  - Materials availability
  - Data and code availability
- EXPERIMENTAL MODEL AND SUBJECT DETAILS
- METHOD DETAILS
  - Plasmids
  - Search for suppressors of the DNA damage sensitivity of *exo1*Δ *sgs1*Δ cells
  - Spot assays
  - DSB resection at the *MAT* locus
  - Protein extract preparation and western blotting
  - Coimmunoprecipitation
  - ONPG assay
  - Chromatin immunoprecipitation and qPCR
  - Prediction of PP2A structure
- QUANTIFICATION AND STATISTICAL ANALYSIS

SUPPLEMENTAL INFORMATION

Supplemental information can be found online at https://doi.org/10.1016/j.celrep.2023.113360.

ACKNOWLEDGMENTS

We thank J. Haber, J. Diffley, and M. Muzi-Falconi for providing yeast strains and plasmids. We are also grateful to E. Gobbini for conducting the genetic

screen, E. Ferrari for assistance with the OA experiment, R. Fraschini for expertise in the two-hybrid assay, R. Tisi for insight into the PP2A structure, and A. Civetta for preliminary data. This work was supported by Fondazione AIRC under IG 2022 - ID. 27001 project - P.I. Maria Pia Longhese and Progetti di Ricerca di Interesse Nazionale (PRIN) 2020 and PRIN 2022, to M.P.L.

AUTHOR CONTRIBUTIONS

Conceptualization, E.C., M.C., and M.P.L.; investigation, E.C., P.P., C.R., and M.G.; writing – original draft, M.P.L.; writing – review & editing, E.C., M.C., and M.P.L.; supervision, M.P.L.; funding acquisition, M.P.L.

DECLARATION OF INTERESTS

The authors declare no competing interests.

Received: June 3, 2023
Revised: September 25, 2023
Accepted: October 13, 2023

REFERENCES

1. Jinks-Robertson, S., and Petes, T.D. (2021). Mitotic recombination in yeast: what we know and what we don't know. Curr. Opin. Genet. Dev. *71*, 78–85.
2. Casari, E., Rinaldi, C., Marsella, A., Gnugnoli, M., Colombo, C.V., Bonetti, D., and Longhese, M.P. (2019). Processing of DNA double-strand breaks by the MRX complex in a chromatin context. Front. Mol. Biosci. *6*, 43.
3. Cannavo, E., and Cejka, P. (2014). Sae2 promotes dsDNA endonuclease activity within Mre11-Rad50-Xrs2 to resect DNA breaks. Nature *514*, 122–125.
4. Mimitou, E.P., and Symington, L.S. (2008). Sae2, Exo1 and Sgs1 collaborate in DNA double-strand break processing. Nature *455*, 770–774.
5. Zhu, Z., Chung, W.H., Shim, E.Y., Lee, S.E., and Ira, G. (2008). Sgs1 helicase and two nucleases Dna2 and Exo1 resect DNA double-strand break ends. Cell *134*, 981–994.
6. Cejka, P., Cannavo, E., Polaczek, P., Masuda-Sasa, T., Pokharel, S., Campbell, J.L., and Kowalczykowski, S.C. (2010). DNA end resection by Dna2-Sgs1-RPA and its stimulation by Top3-Rmi1 and Mre11-Rad50-Xrs2. Nature *467*, 112–116.
7. Niu, H., Chung, W.H., Zhu, Z., Kwon, Y., Zhao, W., Chi, P., Prakash, R., Seong, C., Liu, D., Lu, L., et al. (2010). Mechanism of the ATP-dependent DNA end-resection machinery from *Saccharomyces cerevisiae*. Nature *467*, 108–111.
8. Garcia, V., Phelps, S.E.L., Gray, S., and Neale, M.J. (2011). Bidirectional resection of DNA double-strand breaks by Mre11 and Exo1. Nature *479*, 241–244.
9. Nimonkar, A.V., Genschel, J., Kinoshita, E., Polaczek, P., Campbell, J.L., Wyman, C., Modrich, P., and Kowalczykowski, S.C. (2011). BLM-DNA2-RPA-MRN and EXO1-BLM-RPA-MRN constitute two DNA end resection machineries for human DNA break repair. Genes Dev. *25*, 350–362.
10. Shibata, A., Moiani, D., Arvai, A.S., Perry, J., Harding, S.M., Genois, M.M., Maity, R., van Rossum-Fikkert, S., Kertokalio, A., Romoli, F., et al. (2014). DNA double-strand break repair pathway choice is directed by distinct MRE11 nuclease activities. Mol. Cell *53*, 7–18.
11. Reginato, G., Cannavo, E., and Cejka, P. (2017). Physiological protein blocks direct the Mre11-Rad50-Xrs2 and Sae2 nuclease complex to initiate DNA end resection. Genes Dev. *31*, 2325–2330.
12. Wang, W., Daley, J.M., Kwon, Y., Krasner, D.S., and Sung, P. (2017). Plasticity of the Mre11-Rad50-Xrs2-Sae2 nuclease ensemble in the processing of DNA-bound obstacles. Genes Dev. *31*, 2331–2336.
13. Zou, L., and Elledge, S.J. (2003). Sensing DNA damage through ATRIP recognition of RPA-ssDNA complexes. Science *300*, 1542–1548.
14. Gilbert, C.S., Green, C.M., and Lowndes, N.F. (2001). Budding yeast Rad9 is an ATP-dependent Rad53 activating machine. Mol. Cell *8*, 129–136.
15. Schwartz, M.F., Duong, J.K., Sun, Z., Morrow, J.S., Pradhan, D., and Stern, D.F. (2002). Rad9 phosphorylation sites couple Rad53 to the *Saccharomyces cerevisiae* DNA damage checkpoint. Mol. Cell *9*, 1055–1065.
16. Sweeney, F.D., Yang, F., Chi, A., Shabanowitz, J., Hunt, D.F., and Durocher, D. (2005). *Saccharomyces cerevisiae* Rad9 acts as a Mec1 adaptor to allow Rad53 activation. Curr. Biol. *15*, 1364–1375.
17. Pizzul, P., Casari, E., Gnugnoli, M., Rinaldi, C., Corallo, F., and Longhese, M.P. (2022). The DNA damage checkpoint: A tale from budding yeast. Front. Genet. *13*, 995163.
18. Paciotti, V., Clerici, M., Lucchini, G., and Longhese, M.P. (2000). The checkpoint protein Ddc2, functionally related to S. pombe Rad26, interacts with Mec1 and is regulated by Mec1-dependent phosphorylation in budding yeast. Genes Dev. *14*, 2046–2059.
19. Rouse, J., and Jackson, S.P. (2002). Interfaces between the detection, signaling, and repair of DNA damage. Science (New York, N.Y.) *297*, 547–551.
20. Wang, H., and Elledge, S.J. (2002). Genetic and physical interactions between DPB11 and DDC1 in the yeast DNA damage response pathway. Genetics *160*, 1295–1304.
21. Majka, J., Binz, S.K., Wold, M.S., and Burgers, P.M.J. (2006). Replication protein A directs loading of the DNA damage checkpoint clamp to 5'-DNA junctions. J. Biol. Chem. *281*, 27855–27861.
22. Mordes, D.A., Nam, E.A., and Cortez, D. (2008). Dpb11 activates the Mec1-Ddc2 complex. Proc. Natl. Acad. Sci. USA *105*, 18730–18734.
23. Navadgi-Patil, V.M., and Burgers, P.M. (2008). Yeast DNA replication protein Dpb11 activates the Mec1/ATR checkpoint kinase. J. Biol. Chem. *283*, 35853–35859.
24. Navadgi-Patil, V.M., and Burgers, P.M. (2009). The unstructured C-terminal tail of the 9-1-1 clamp subunit Ddc1 activates Mec1/ATR via two distinct mechanisms. Mol. Cell *36*, 743–753.
25. Puddu, F., Granata, M., Di Nola, L., Balestrini, A., Piergiovanni, G., Lazzaro, F., Giannattasio, M., Plevani, P., and Muzi-Falconi, M. (2008). Phosphorylation of the budding yeast 9-1-1 complex is required for Dpb11 function in the full activation of the UV-induced DNA damage checkpoint. Mol. Cell Biol. *28*, 4782–4793.
26. Pfander, B., and Diffley, J.F.X. (2011). Dpb11 coordinates Mec1 kinase activation with cell cycle-regulated Rad9 recruitment. EMBO J. *30*, 4897–4907.
27. Delacroix, S., Wagner, J.M., Kobayashi, M., Yamamoto, K.i., and Karnitz, L.M. (2007). The Rad9-Hus1-Rad1 (9-1-1) clamp activates checkpoint signaling via TopBP1. Genes Dev. *21*, 1472–1477.
28. Lazzaro, F., Sapountzi, V., Granata, M., Pellicioli, A., Vaze, M., Haber, J.E., Plevani, P., Lydall, D., and Muzi-Falconi, M. (2008). Histone methyltransferase Dot1 and Rad9 inhibit single-stranded DNA accumulation at DSBs and uncapped telomeres. EMBO J. *27*, 1502–1512.
29. Clerici, M., Trovesi, C., Galbiati, A., Lucchini, G., and Longhese, M.P. (2014). Mec1/ATR regulates the generation of single-stranded DNA that attenuates Tel1/ATM signaling at DNA ends. EMBO J. *33*, 198–216.
30. Ngo, G.H.P., and Lydall, D. (2015). The 9-1-1 checkpoint clamp coordinates resection at DNA double strand breaks. Nucleic Acids Res. *43*, 5017–5032.
31. Bonetti, D., Villa, M., Gobbini, E., Cassani, C., Tedeschi, G., and Longhese, M.P. (2015). Escape of Sgs1 from Rad9 inhibition reduces the requirement for Sae2 and functional MRX in DNA end resection. EMBO Rep. *16*, 351–361.
32. Ferrari, M., Dibitetto, D., De Gregorio, G., Eapen, V.V., Rawal, C.C., Lazzaro, F., Tsabar, M., Marini, F., Haber, J.E., and Pellicioli, A. (2015). Functional interplay between the 53BP1-ortholog Rad9 and the Mre11 complex regulates resection, end-tethering and repair of a double-strand break. PLoS Genet. *11*, e1004928.

33. Yu, T.Y., Kimble, M.T., and Symington, L.S. (2018). Sae2 antagonizes Rad9 accumulation at DNA double-strand breaks to attenuate checkpoint signaling and facilitate end resection. Proc. Natl. Acad. Sci. USA *115*, E11961–E11969.

34. Bantele, S.C.S., Lisby, M., and Pfander, B. (2019). Quantitative sensing and signalling of single-stranded DNA during the DNA damage response. Nat. Commun. *10*, 944.

35. Gobbini, E., Casari, E., Colombo, C.V., Bonetti, D., and Longhese, M.P. (2020). The 9-1-1 complex controls Mre11 nuclease and checkpoint activation during short-range resection of DNA double-strand breaks. Cell Rep. *33*, 108287.

36. Ellison, V., and Stillman, B. (2003). Biochemical characterization of DNA damage checkpoint complexes: clamp loader and clamp complexes with specificity for 5' recessed DNA. PLoS Biol. *1*, E33.

37. Majka, J., and Burgers, P.M.J. (2003). Yeast Rad17/Mec3/Ddc1: a sliding clamp for the DNA damage checkpoint. Proc. Natl. Acad. Sci. USA *100*, 2249–2254.

38. Vaze, M.B., Pellicioli, A., Lee, S.E., Ira, G., Liberi, G., Arbel-Eden, A., Foiani, M., and Haber, J.E. (2002). Recovery from checkpoint-mediated arrest after repair of a double-strand break requires Srs2 helicase. Mol. Cell *10*, 373–385.

39. Tercero, J.A., Longhese, M.P., and Diffley, J.F.X. (2003). A central role for DNA replication forks in checkpoint activation and response. Mol. Cell *11*, 1323–1336.

40. Leroy, C., Lee, S.E., Vaze, M.B., Ochsenbein, F., Guerois, R., Haber, J.E., and Marsolier-Kergoat, M.C. (2003). PP2C phosphatases Ptc2 and Ptc3 are required for DNA checkpoint inactivation after a double-strand break. Mol. Cell *11*, 827–835.

41. Guillemain, G., Ma, E., Mauger, S., Miron, S., Thai, R., Guérois, R., Ochsenbein, F., and Marsolier-Kergoat, M.C. (2007). Mechanisms of checkpoint kinase Rad53 inactivation after a double-strand break in *Saccharomyces cerevisiae*. Mol. Cell Biol. *27*, 3378–3389.

42. Bazzi, M., Mantiero, D., Trovesi, C., Lucchini, G., and Longhese, M.P. (2010). Dephosphorylation of gamma H2A by Glc7/protein phosphatase 1 promotes recovery from inhibition of DNA replication. Mol. Cell Biol. *30*, 131–145.

43. O'Neill, B.M., Szyjka, S.J., Lis, E.T., Bailey, A.O., Yates, J.R., 3rd, Aparicio, O.M., and Romesberg, F.E. (2007). Pph3-Psy2 is a phosphatase complex required for Rad53 dephosphorylation and replication fork restart during recovery from DNA damage. Proc. Natl. Acad. Sci. USA *104*, 9290–9295.

44. Szyjka, S.J., Aparicio, J.G., Viggiani, C.J., Knott, S., Xu, W., Tavaré, S., and Aparicio, O.M. (2008). Rad53 regulates replication fork restart after DNA damage in *Saccharomyces cerevisiae*. Genes Dev. *22*, 1906–1920.

45. Travesa, A., Duch, A., and Quintana, D.G. (2008). Distinct phosphatases mediate the deactivation of the DNA damage checkpoint kinase Rad53. J. Biol. Chem. *283*, 17123–17130.

46. Kim, J.A., Hicks, W.M., Li, J., Tay, S.Y., and Haber, J.E. (2011). Protein phosphatases Pph3, Ptc2, and Ptc3 play redundant roles in DNA double-strand break repair by homologous recombination. Mol. Cell Biol. *31*, 507–516.

47. Hustedt, N., Seeber, A., Sack, R., Tsai-Pflugfelder, M., Bhullar, B., Vlaming, H., van Leeuwen, F., Guénolé, A., van Attikum, H., Srivas, R., et al. (2015). Yeast PP4 interacts with ATR homolog Ddc2-Mec1 and regulates checkpoint signaling. Mol. Cell *57*, 273–289.

48. Falk, J.E., Chan, A.C.h., Hoffmann, E., and Hochwagen, A. (2010). A Mec1- and PP4-dependent checkpoint couples centromere pairing to meiotic recombination. Dev. Cell *19*, 599–611.

49. Zhang, W., and Durocher, D. (2010). De novo telomere formation is suppressed by the Mec1-dependent inhibition of Cdc13 accumulation at DNA breaks. Genes Dev. *24*, 502–515.

50. Bandyopadhyay, S., Chiang, C.Y., Srivastava, J., Gersten, M., White, S., Bell, R., Kurschner, C., Martin, C.H., Smoot, M., Sahasrabudhe, S., et al. (2010). A human MAP kinase interactome. Nat. Methods *7*, 801–805.

51. Keogh, M.C., Kim, J.A., Downey, M., Fillingham, J., Chowdhury, D., Harrison, J.C., Onishi, M., Datta, N., Galicia, S., Emili, A., et al. (2006). A phosphatase complex that dephosphorylates gammaH2AX regulates DNA damage checkpoint recovery. Nature *439*, 497–501.

52. Ferrari, E., Bruhn, C., Peretti, M., Cassani, C., Carotenuto, W.V., Elgendy, M., Shubassi, G., Lucca, C., Bermejo, R., Varasi, M., et al. (2017). PP2A controls genome integrity by integrating nutrient-sensing and metabolic pathways with the DNA damage response. Mol. Cell *67*, 266–281.e4.

53. Dozier, C., Bonyadi, M., Baricault, L., Tonasso, L., and Darbon, J.M. (2004). Regulation of Chk2 phosphorylation by interaction with protein phosphatase 2A via its B' regulatory subunit. Biol. Cell *96*, 509–517.

54. Goodarzi, A.A., Jonnalagadda, J.C., Douglas, P., Young, D., Ye, R., Moorhead, G.B.G., Lees-Miller, S.P., and Khanna, K.K. (2004). Autophosphorylation of ataxia-telangiectasia mutated is regulated by protein phosphatase 2A. EMBO J. *23*, 4451–4461.

55. Chowdhury, D., Keogh, M.C., Ishii, H., Peterson, C.L., Buratowski, S., and Lieberman, J. (2005). gamma-H2AX dephosphorylation by protein phosphatase 2A facilitates DNA double-strand break repair. Mol. Cell *20*, 801–809.

56. Leung-Pineda, V., Ryan, C.E., and Piwnica-Worms, H. (2006). Phosphorylation of Chk1 by ATR is antagonized by a Chk1-regulated protein phosphatase 2A circuit. Mol. Cell Biol. *26*, 7529–7538.

57. Petersen, P., Chou, D.M., You, Z., Hunter, T., Walter, J.C., and Walter, G. (2006). Protein phosphatase 2A antagonizes ATM and ATR in a Cdk2- and Cdc7-independent DNA damage checkpoint. Mol. Cell Biol. *26*, 1997–2011.

58. Kalev, P., Simicek, M., Vazquez, I., Munck, S., Chen, L., Soin, T., Danda, N., Chen, W., and Sablina, A. (2012). Loss of PPP2R2A inhibits homologous recombination DNA repair and predicts tumor sensitivity to PARP inhibition. Cancer Res. *72*, 6414–6424.

59. Moyano-Rodriguez, Y., and Queralt, E. (2019). PP2A functions during mitosis and cytokinesis in yeasts. Int. J. Mol. Sci. *21*, 264.

60. Amin, P., Awal, S., Vigneron, S., Roque, S., Mechali, F., Labbé, J.C., Lorca, T., and Castro, A. (2022). PP2A-B55: substrates and regulators in the control of cellular functions. Oncogene *41*, 1–14.

61. Lee, S.E., Moore, J.K., Holmes, A., Umezu, K., Kolodner, R.D., and Haber, J.E. (1998). *Saccharomyces* Ku70, Mre11/Rad50 and RPA proteins regulate adaptation to G2/M arrest after DNA damage. Cell *94*, 399–409.

62. Gnugnoli, M., Casari, E., and Longhese, M.P. (2021). The chromatin remodeler Chd1 supports MRX and Exo1 functions in resection of DNA double-strand breaks. PLoS Genet. *17*, e1009807.

63. Guo, X., Hum, Y.F., Lehner, K., and Jinks-Robertson, S. (2017). Regulation of hetDNA length during mitotic double-strand break repair in yeast. Mol. Cell *67*, 539–549.e4.

64. Zhang, Z., Mui, M.Z., Chan, F., Roopchand, D.E., Marcellus, R.C., Blanchette, P., Li, S., Berghuis, A.M., and Branton, P.E. (2011). Genetic analysis of B55alpha/Cdc55 protein phosphatase 2A subunits: association with the adenovirus E4orf4 protein. J. Virol. *85*, 286–295.

65. Groves, M.R., Hanlon, N., Turowski, P., Hemmings, B.A., and Barford, D. (1999). The structure of the protein phosphatase 2A PR65/A subunit reveals the conformation of its 15 tandemly repeated HEAT motifs. Cell *96*, 99–110.

66. Evans, R., O'Neill, M., Pritzel, A., Antropova, N., Senior, A., Green, T., Žídek, A., Bates, R., Blackwell, S., Yim, J., et al. (2021). Protein complex prediction with AlphaFold-Multimer. Preprint at bioRxiv. https://doi.org/10.1101/2021.10.04.463034.

67. Longhese, M.P., Paciotti, V., Fraschini, R., Zaccarini, R., Plevani, P., and Lucchini, G. (1997). The novel DNA damage checkpoint protein Ddc1p is phosphorylated periodically during the cell cycle and in response to DNA damage in budding yeast. EMBO J. *16*, 5216–5226.

68. Ishihara, H., Martin, B.L., Brautigan, D.L., Karaki, H., Ozaki, H., Kato, Y., Fusetani, N., Watabe, S., Hashimoto, K., Uemura, D., et al. (1989). Calyculin A and okadaic acid: inhibitors of protein phosphatase activity. Biochem. Biophys. Res. Commun. *159*, 871–877.

69. Mestrović, V., and Pavela-Vrancic, M. (2003). Inhibition of alkaline phosphatase activity by okadaic acid, a protein phosphatase inhibitor. Biochimie *85*, 647–650.

70. Xu, Y., Xing, Y., Chen, Y., Chao, Y., Lin, Z., Fan, E., Yu, J.W., Strack, S., Jeffrey, P.D., and Shi, Y. (2006). Structure of protein phosphatase 2A core enzyme bound to tumor-inducing toxins. Cell *127*, 1239–1251.

71. Casari, E., Gobbini, E., Clerici, M., and Longhese, M.P. (2021). Resection of a DNA double-strand break by alkaline gel electrophoresis and southern blotting. Methods Mol. Biol. *2153*, 33–45.

72. Casari, E., Gobbini, E., Gnugnoli, M., Mangiagalli, M., Clerici, M., and Longhese, M.P. (2021). Dpb4 promotes resection of DNA double-strand breaks and checkpoint activation by acting in two different protein complexes. Nat. Commun. *12*, 4750.

STAR★METHODS

KEY RESOURCES TABLE

REAGENT or RESOURCE	SOURCE	IDENTIFIER
Antibodies		
Anti-Rad53	Abcam	Cat#Ab104232; RRID: AB_2687603
Anti-HA (12CA5)	In house	N/A
Anti-Myc (9E10)	Abcam	Cat#Ab32; RRID: AB_303599
Bacterial and Virus Strains		
Subcloning Efficiency™ DH5alpha Competent Cells	Invitrogen	Cat#18265017
Chemicals, peptides, and recombinant proteins		
Sspl-HF	NEB	Cat#R3132L
SsoFast EvaGreen Supermix, 500 Rxn	Bio-Rad	Cat#1725201
Hygromycin B	Roche	Cat#10843555001
ClonNAT (nourseothricin)	Jena Bioscience	Cat#AB-102
G-418 disulfate	Merck	Cat#A1720
Phleomycin	Merck	Cat#P9564-100MG
(S)-(+)-Camptothecin	Merck	Cat#C9911-1G
Zymolyase 20T	Nacalai Tesque	Cat#07663-91
Zymolyase 100T	Nacalai Tesque	Cat#0766555
EASYTIDES UTP [alpha-32P]	Perkin Elmer	Cat#NEG507T250UC
Dynabeads Protein G	Invitrogen	Cat#10004D
D(+)-Raffinose pentahydrate	Merck	Cat#83400-100G
D(+)-Galactose	Merck	Cat#48260-500G-F
D(+)-Glucose monohydrate	Merck	Cat#49159-5KG
Yeast Extract Difco	BD	Cat#212750
Peptone DIFCO	BD	Cat#211677
Peptone Oxoid	OXOID	Cat#LP0037T
Yeast extract Oxoid	OXOID	Cat#LP0021T
Agar Bacto Difco	BD	Cat#214030
Agarose LE	EuroClone	Cat#EMR920500
TAE buffer (50X)	EuroClone	Cat#APA16911000
Methanol	Merck	Cat#179337-2.5L
Trichloroacetic acid	Merck	Cat#91230-1KG
RNase A	Roche	Cat#10109169001
Bromophenol Blue sodium salt	Merck	Cat#B6131-25G
Phenylmethanesulfonyl fluoride	Merck	Cat#78830-5G
tRNA	Roche	Cat#10109495001
Sodium Chloride	Merck	Cat#31434-M
Formamide	Merck	Cat#47671-1L-F
Denhardt's Solution 50x	Merck	Cat#D2532-5X5ML
2-Nitrophenyl β-D-galactopyranoside	Merck	Cat#N1127-1G
Ficoll® PM 400	Merck	Cat#F4375-25G
Triton® X-100 for molecular biology	Merck	Cat#T8787-100ML
Dimethyl sulfoxide	Merck	Cat#D4540-1L
SSPE buffer 20X concentrate	Merck	Cat#S2015-1L
Deoxyribonucleic acid, single stranded from salmon testes	Merck	Cat#D7656-5X1ML

(*Continued on next page*)

Continued

REAGENT or RESOURCE	SOURCE	IDENTIFIER
Yeast nitrogen base with amino acids	Merck	Cat#Y1250-250G
Hydrochloric acid	Merck	Cat#30721-1L-M
Ethanol absolute	Merck	Cat#02860-2.5L
Ammonium persulfate	Merck	Cat#A3678-25G
IGEPAL® CA-630	Merck	Cat#I8896-100ML
N,N,N′,N′-Tetramethylethylenediamine	Merck	Cat#T9281-50ML
Dextran sulfate sodium salt from *Leuconostoc* spp	Merck	Cat#D8906-100G
Lithium chloride	Merck	Cat#L9650-100G
Sodium deoxycholate	Merck	Cat#30970-100G
Acrylamide 4X solution	Serva	Cat#10677.1
N,N′-Methylene-bisacrylamide 2X	Serva	Cat#29197.01
2-Propanol	Merck	Cat#I9516-500ML
Glycine for electrophoresis, ≥99%	Merck	Cat#G8898-1KG
Formaldehyde solution for molecular biology, 36.5–38% in H2O	Merck	Cat#F8775-500ML
Sodium hydroxide	Merck	Cat#1064621000
Sodium dodecyl sulfate	Merck	Cat#L3771-500G
Trizma® base	Merck	Cat#33742-2KG
Ponceau s sodium practical grade	Merck	Cat#P3504-100G
D-Sorbitol	Merck	Cat#S7547-1KG
Complete Mini	Roche	Cat#11836153001
Ethylenediaminetetraacetic acid ≥98.0%	Merck	Cat#03620-1KG
HEPES	Merck	Cat#H4034-1KG
DL-Dithiothreitol	Merck	Cat#43819-25G
Calcium carbonate	Merck	Cat#239216
Potassium chloride	Merck	Cat#P3911
Sodium phosphate dibasic	Merck	Cat#S9763
Potassium phosphate monobasic	Merck	Cat#P0662
Bio-Rad Protein Assay Dye Reagent Concentrate	Bio-Rad	Cat#5000006
Sodium orthovanadate	Merck	Cat#S6508-10G
β-Glycerophosphate disodium salt hydrate	Merck	Cat#G9422
Clarity Western ECL Substrate	Bio-Rad	Cat#1705061
Okadaic Acid	Merck	Cat#495604
Critical commercial assays		
Riboprobe System-T7	Promega	Cat#P1440
QIAGEN QIAquick PCR Purification Kit	QIAGEN	Cat#28106
QIAquick Gel Extraction Kit	QIAGEN	Cat#28704
QIAprep Spin Miniprep Kit	QIAGEN	Cat#27104
Experimental Models: Organisms/Strains		
S. cerevisiae, see Table S1	This paper	N/A
Oligonucleotides		
ARO+: TGAGTCGTTACAAGGTGATGCC	This paper	N/A
ARO-: ACCTACAGGAGGACCCGAAA	This paper	N/A
DSB 0.6+: CACCCAAGAAGGCGAATAAG	This paper	N/A
DSB 0.6-: CATGCGGTTCACATGACTTT	This paper	N/A
DSB 1.8+: ACGTCGTTGTTAATGGTGGTG	This paper	N/A
DSB 1.8-: CGCGAGTCTTATGCCAAAAA	This paper	N/A

(*Continued on next page*)

Continued

REAGENT or RESOURCE	SOURCE	IDENTIFIER
Software and algorithms		
Bio-Rad CFX Maestro 1.1 Version: 4.1.2433.1219	Bio-Rad	N/A
Scion Image Beta 4.0.2	Scion Corporation	N/A
Other		
Primo® FrameStar® 96well PCR Plate, semi-skirted, clear wells	Euroclone	Cat#ECPCR0770C
HYBOND-NX Nylon membrane	GE Healthcare	Cat#GEHRPN203T
Nitrocellulose blotting membrane, Amersham™ Protran™ 0.45 μm NC	GE Healthcare	Cat#GEH10600002
Hyperfilm MP	GE Healthcare	Cat#GEH28906844

RESOURCE AVAILABILITY

Lead contact

Further information and requests for resources and reagents should be directed to and will be fulfilled by the lead contact, Maria Pia Longhese (mariapia.longhese@unimib.it).

Materials availability

All unique/stable reagents generated in this study are available from the lead contact without restriction.

Data and code availability

- All data reported in this paper will be shared by the lead contact upon request.
- This paper does not report original datasets or code.
- Any additional information required to reanalyze the data reported in this paper is available from the lead contact upon request.

EXPERIMENTAL MODEL AND SUBJECT DETAILS

Saccharomyces cerevisiae is the experimental model used in this study. Strain genotypes are listed in Table S1. Strain JKM139, used to detect DSB resection, was kindly provided by J. Haber (Brandeis University, Waltham, USA). The *ddc1-T602A* allele was kindly provided by J. Diffley (The Francis Crick Institute, London, UK). The strain EGY48, used to perform the ONPG assay, was kindly provided by M. Muzi-Falconi (University of Milan, Milan, Italy). Gene disruptions and tag fusions were constructed by one-step PCR homology cassette amplification and standard yeast transformation methods. Cells were grown in YEP medium (1% yeast extract, 2% bactopeptone) supplemented with 2% glucose (YEPD), 2% raffinose (YEPR) or 2% raffinose and 3% galactose (YEPRG). All the experiments have been performed at 25°C.

METHOD DETAILS

Plasmids

To perform the ONPG assay, plasmids pFP1 (pJG4-5-*DPB11*), pFP2 (pEG202-*DDC1*), pJG4-5, pEG202, and β-gal reporter pSH18-34 were kindly provided by M. Muzi-Falconi (University of Milan, Milan, Italy). Plasmid pML796.3 (pEG202-*ddc1-T602A*) was generated in this study.

Search for suppressors of the DNA damage sensitivity of *exo1*Δ *sgs1*Δ cells

The search for suppressor mutations of the DNA damage sensitivity of *exo1*Δ *sgs1*Δ cells was previously described.[35] Briefly, $5x10^6$ *exo1*Δ *sgs1*Δ cells were plated on YEPD in the presence of CPT or phleomycin. Survivors were crossed to wild-type cells to identify by tetrad analysis the suppression events that were due to single-gene mutations. Genomic DNA from single-gene suppressors was analyzed by next-generation Illumina sequencing (IGA technology services). To confirm that the *cdc55-Q335E* and *tpd3-I384N* alleles were responsible for the suppression, the *HPHMX* and *NATMX* genes were integrated downstream of the *cdc55-Q335E* and *tpd3-I384N* stop codon, respectively, and the resulting strain was crossed to wild-type cells to verify by tetrad dissection that the suppression of the *exo1*Δ *sgs1*Δ sensitivity co-segregated with the *HPHMX* and *NATMX* markers.

Spot assays

Cells grown overnight were diluted to 1x10^7 cells/ml. 10-fold serial dilutions were spotted on YEPD with or without indicated DNA damaging drugs. Plates were incubated for 3 days at 25°C.

DSB resection at the *MAT* locus

DSB end resection at the *MAT* locus in JKM139 derivative strains was analyzed on alkaline agarose gels, by using a single-stranded probe complementary to the unresected DSB strand, as previously described.[71] Quantitative analysis of DSB resection was performed by calculating the ratio of band intensities for ssDNA and total amount of DSB products. The resection efficiency was normalized with respect to the HO cleavage efficiency for each time point. Densitometric analysis of band intensities was performed using Scion Image Beta 4.0.2 software. Quantitative PCR (qPCR) analysis of DSB resection at the *MAT* locus in JKM139 derivative strains was carried out as previously described.[62] Genomic DNA was extracted at different time points following HO induction and digested with both *Ssp*I and *Rsa*I restriction enzymes. A mock reaction without the restriction enzymes was set up in parallel. qPCR was performed on both digested and mock samples with oligonucleotides that anneal at specific distances from the DSB and using SsoFast EvaGreen supermix (Bio-Rad) on the Bio-Rad CFX Connect Real-Time System apparatus. For each time point, Ct values were normalized to those obtained from the mock sample, and then further normalized to values obtained from an amplicon in the *KCC4* control gene. The obtained values were normalized to the HO-cut efficiency measured by qPCR by using oligonucleotides that anneal on opposite sides with respect to the HO cutting sequence. The percentage of HO-cut was calculated by comparing the Ct values before and after HO induction in undigested samples.

Protein extract preparation and western blotting

Protein extracts for western blot analysis were prepared by trichloroacetic acid (TCA) precipitation. Frozen cell pellets were resuspended in 100 μL 20% TCA. After the addition of acid-washed glass beads, the samples were vortexed for 10 min. The beads were washed with 400 μL of 5% TCA, and the extract was collected in a new tube. The crude extract was precipitated by centrifugation at 3000 rpm for 10 min. TCA was discarded, and samples were resuspended in 70 μL 2X Laemmli buffer (60mM Tris, pH 6.8, 2% SDS, 10% glycerol, 100mM DTT, 0.2% bromophenol blue) containing 0.9% β-mercaptoethanol and 30 μL 1M Tris (pH 8.0). Prior to loading, samples were boiled at 99°C and centrifuged at 3000 rpm for 10 min. Supernatant containing the solubilized proteins were separated on 10% polyacrylamide gels. Rad53 was detected by using anti-Rad53 polyclonal antibodies (ab104232) (1:2000) from Abcam. HA-tagged proteins were detected by using an anti-HA (12CA5) (1:2000) antibody. Images were collected using the ChemiDoc (Bio-Rad) and ImageLab software.

Coimmunoprecipitation

Total protein extracts were prepared by breaking cells in 400 μL of buffer containing 0.1% SDS, 1% Triton X-100, 1% Nadeoxycholate, 0.05M Tris–HCl pH 7.5, 1mM phenylmethylsulfonyl, 1mM sodium orthovanadate, 60mM β-glycerophosphate and protease inhibitor cocktail (Roche Diagnostics), as previously described.[67] An equal volume of breaking buffer was added to clarified protein extracts and tubes were incubated for 2 h at 4°C with 50 μL of Protein G-Dynabeads and 5 μg of an anti-HA (12CA5) antibody. The resins were then washed three times with 1 mL PBS 1X. Bound proteins were visualized by western blotting with an anti-HA (12CA5) (1:2000) or anti-Myc (9E10) (1:1000) antibody after electrophoresis on a 10% SDS-polyacrylamide gel.

ONPG assay

Enzyme activity of β-galactosidase was measured by using *ortho*-nitrophenyl-β-galactoside (ONPG) substrate. After cells breaking, the assay was performed at 37°C in PBS buffer 1X pH 7.4. After 3 min, the reaction was stopped by adding an equal volume of 1M pH 11 sodium carbonate buffer. The absorbance was detected at 420 nm with a UV/VIS spectrophotometer. One unit of β-galactosidase enzyme activity was measured as the quantity of the enzyme that catalyzes the production of 1 μmol of ONPG per minute. The β-galactosidase activity was normalized dividing the Enzyme Unit (U) by the total proteins (mg).

Chromatin immunoprecipitation and qPCR

ChIP analysis was performed as previously described.[72] Quantification of immunoprecipitated DNA was achieved by quantitative real-time PCR (qPCR) on a Bio-Rad CFX Connect Real-Time System apparatus and Bio-Rad CFX Maestro 1.1 software. Triplicate samples in 20 μL reaction mixture containing 10 ng of template DNA, 300nM for each primer, 2x SsoFast EvaGreen supermix (Bio-Rad #1725201) (2x reaction buffer with dNTPs, Sso7d-fusion polymerase, $MgCl_2$, EvaGreen dye, and stabilizers) were run in white 96-well PCR plates Multiplate (Bio-Rad #MLL9651). The qPCR program was as follows: step 1, 98°C for 2 min; step 2, 90°C for 5 s; step 3, 60°C for 15 s; step 4, return to step 2 and repeat 45 times. At the end of the cycling program, a melting program (from 65°C to 95°C with a 0.5°C increment every 5 s) was run to test the specificity of each qPCR. Data are expressed as fold enrichment at the HO-induced DSB over that at the non-cleaved *ARO1* locus, after normalization of each ChIP signal to the corresponding input for each time point. Fold enrichment was then normalized to the efficiency of DSB induction.

Prediction of PP2A structure

Alphafold2-Multimer[66] was used for the prediction of the tetrameric complex of PP2A phosphatase. Default settings were kept for MSA, using the MMseqs2 clustering module, while template search was disabled and the number of recycles was set on three.

QUANTIFICATION AND STATISTICAL ANALYSIS

Data are expressed as mean values ±standard deviation. Statistical analyses were performed using Microsoft Excel Professional 365 software. p values were determined by using an unpaired two-tailed t test. No statistical methods or criteria were used to estimate sample size or to include or exclude samples.